Journal of Sound and Vibration (1997) **202**(1), 29–46

VIBRATION CHARACTERISTICS OF A SUSPENSION FOOTBRIDGE

J. M. W. BROWNJOHN

School of Civil and Structural Engineering, *Nanyang Technological University*, *Nanyang Avenue*, *Singapore* 639798, *Republic of Singapore*

(*Received* 28 *October* 1995, *and in final form* 12 *August* 1996)

A suspension footbridge located in a tourist attraction in Singapore has a suspended span of 35 m and was designed for static pedestrian and wind loads. In common with other bridges of this type, it is a light, efficient structure and has a lively dynamic performance.

Distributed parameter and finite element models were used to understand the vertical plane behaviour of the bridge and a prototype dynamic test using impact excitation was conducted to check the models and investigate the dynamic response.

The first two vertical vibration modes were found to occur at the same frequency, 2 Hz, as the average pedestrian footfall. Response to pedestrians was simulated using linear and non-linear models of a moving excitation source.

1. INTRODUCTION

At the time of writing, the only conventional suspension bridge in service in Singapore is a 35 m span footbridge located in a tourist attraction. Because such a bridge is unusual in Singapore, the design was made to be conservative, but the bridge has quite a lively dynamic response. This "bouncy" bridge is seen as a positive asset, adding to the attraction to visitors. The liveliness is typical of cable supported footbridges [1, 2].

Preliminary dynamic investigations from impact testing, heel drop and heavy walking indicated that vertical vibrations were readily excited, lateral vibrations could only be excited with difficulty, and that torsional response was generated only by deliberate effort and was heavily damped.

It was found that vertical plane vibrations at approximately 2 Hz could be excited as an antisymmetric mode or a symmetric mode depending on the point of excitation. A single person walking heavily across the bridge could excite noticeable vibrations at this frequency before reaching mid-span, resulting in a "floating" sensation while walking across the remaining half-span. The nature of the 2 Hz vertical plane performance was therefore of particular interest due to its coincidence with the natural footfall frequency.

The aim of this research has been: (a) to explore the liveliness of the bridge experimentally; (b) to set up simple mathematical models representing vertical plane performance; (c) to explore effects of varying structural parameters and tune the models to the experimental results; and (d) to compare the measured response to a pedestrian with simulation from linear and non-linear models.

2. STRUCTURAL ARRANGEMENT

The bridge features are shown in Figure 1. The suspended deck has a 35 m span and there are no side spans. The deck comprises three grade 43 229 × 89 mm rolled steel

0022–460X/97/160029 + 18 $25.00/0/sv960789

channel section stringers with total second moment of area $I = 1{\cdot}02 \times 10^8$ mm^4. Lateral bracing is provided by 152 × 76 mm channel section transom beams welded below the stringers at 3 m intervals. 70 × 70 mm angles span diagonally between transoms. The walkway comprises 25 mm timber panels supported on the stringers. The handrail system is a vertical unbraced steel frame with uprights welded to the transoms.

The towers comprise rolled steel square and rectangular hollow sections. Each tower upright, 6 m high, is braced by two diagonal and two horizontal members and is pinned about a lateral axis at the tower footing. Curved machined blocks form the saddles. Each main cable is a 26 mm diameter fibre core wire rope with a sag of 5·5 m and a horizontal tension of approximately 30 kN per cable. In the design for static loads the effective cable area A_c and (static) modulus E_c were taken as 66% and 30% respectively of values for solid steel material. The straight backstays are 9·4 m long, at 30° to the horizontal. Vertical hangers, at 3 m intervals, are 16 mm diameter steel rods, effectively pinned at each end.

The fixity at the end of the deck is uncertain; the deck stringers end at the tower footings, without specific restraint. The handrails continue beyond the towers and offer some restraint to rotation.

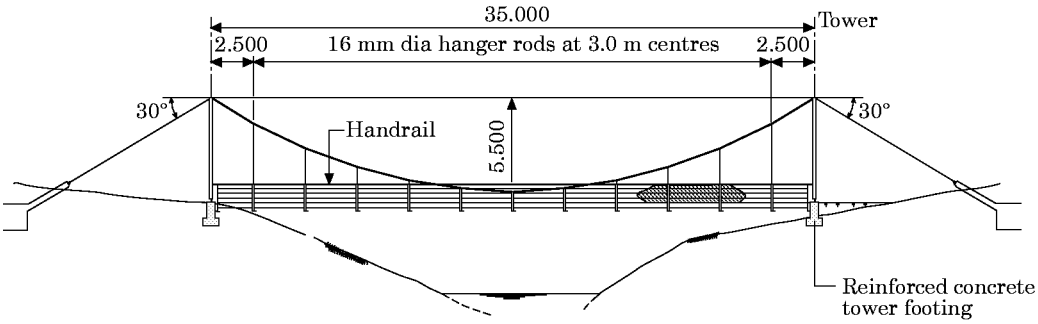

General elevation of bridge

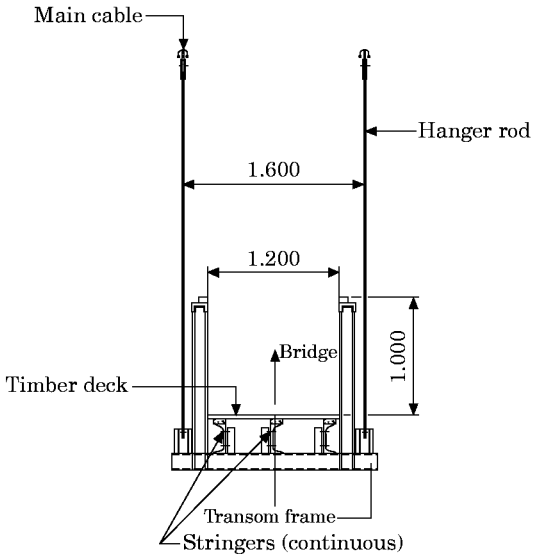

Figure 1. The general arrangement of the suspension footbridge.

The design of the structure, for static loading, was for 31 m/s wind speed, an unfactored dead load of 2·14 kN/m and an unfactored live load of 5·58 kN/m.

3. MATHEMATICAL LOADING

From preliminary experimental investigations of the behaviour of the bridge, which included excitation by heel-drop, walking and bouncing, it was observed that the vertical plane vibrations were the strongest, most interesting and important aspect of the dynamic behaviour. From the experience of analyzing and testing several other suspension bridges [2–5], it is clear that the behaviour in the vertical plane is usually modelled with acceptable accuracy using two-dimensional models, taking the deck as a beam. This particular bridge has many similarities with the previously tested bridges; it is symmetric, with cables and hangers in parallel vertical planes. The torsional and lateral resistance of the deck in the other bridges has little, if any, effect on the vertical plane behaviour.

Since the design of the bridge for static loads is conservative, the deck is likely to contribute significantly to the dynamic stiffness. In the complete suspension bridge, since the hangers are stiff, the deck and cable are forced to vibrate together in the vertical plane. As separate components, the deck and cable would adopt their own vibration patterns, so it is interesting to see to what extent the marriage of the deck and cable modifies the natural behaviour of each substructure. To this end the bridge was represented as (i) a catenary (i.e., zero deck rigidity), (ii) a beam (i.e., zero cable tension) and (iii) bridge—a combination of beams (girders) suspended from the catenary.

Each of these was modelled as a distributed parameter (DP) system using continuum equations and the bridge was also modelled using discrete co-ordinates or finite elements (FEs). In each case the total mass and stiffness characteristics were collapsed to a single vertical plane representation, ignoring lateral and torsional behaviour.

4. CONTINUUM EQUATIONS FOR THE DISTRIBUTED PARAMETER SYSTEM

For the catenary, the ends are assumed to be fixed and the mass of the deck is assumed to be directly transmitted to the cable by inextensible connections. The total load per unit length is ρ. In the static configuration the horizontal component of cable tension is H; the time varying part in dynamic response is $h(t)$. The vertical position with respect to an origin $(x, y = 0)$ at the lowest (mid-span) point in the cable is $y(x)$ and the time varying part is $v(x, t)$.

Under static loads, equilibrium is given by

$$Hy'' = \rho \tag{1}$$

and for dynamic response in free vibration by

$$(H + h)(y + v)'' = \rho + \rho\ddot{v}/g. \tag{2}$$

Combining equations (1) and (2), ignoring second order terms, using the mid-span sag computed from equation (1), $d = \rho l^2/8H$, and using a term $-EIv^{iv}$ for girder rigidity leads to the following:

catenary,
$$v'' - \frac{\ddot{v}\rho}{Hg} = -\frac{8dh}{Hl^2}; \tag{3a}$$

TABLE 1

Natural frequencies according to structure and end fixity

		Pinned, $v'' = 0$	Sprung, $v'' = k_r v'$	Clamped, $v' = 0$
f_{VS1} (Hz)	Cable	0·672	—	—
	Beam	0·396	—	0·898
	Bridge (DP)	1·682	1·750	1·771
	Bridge (2-D FE)	1·687	1·755	1·772
	Bridge (3-D FE)	1·634	—	1·726
f_{VA1} (Hz)	Cable	0·472	—	—
	Beam	1·585	—	2·476
	Bridge (DP)	1·654	2·313	2·528
	Bridge (2-D FE)	1·647	2·282	2·490
	Bridge (3-D FE)	1·654	—	2·491

beam,
$$-\frac{\ddot{v}\rho}{g} - EIv^{iv} = 0; \tag{3b}$$

bridge,
$$v'' - \frac{\ddot{v}\rho}{Hg} - \frac{EIv^{iv}}{H} = -\frac{8dh}{Hl^2}. \tag{3c}$$

Assuming a solution of the form $v(x, t) = \hat{v}(x)\, e^{i\omega t}$, $h(t) = \hat{h}\, e^{i\omega t}$ and defining $\beta^2 = \rho\omega^2/Hg$ with $\omega = 2\pi f$, the general solution for equation (3c) is

$$\hat{v}(x) = A \cosh(p_1 x) + B \sinh(p_1 x) + C \cos(p_2 x) + D \sin(p_2 x) - 8d\hat{h}/(\beta l)^2 H, \tag{4}$$

where p_1 and p_2 are

$$p_1 = \left[\frac{(1+\varepsilon)^{1/2} + 1}{2\alpha}\right]^{1/2}, \qquad p_2 = \left[\frac{(1+\varepsilon)^{1/2} - 1}{2\alpha}\right]^{1/2}, \tag{5}$$

$\alpha = EI/H$ and $\varepsilon = 4\alpha\beta^2$. The natural frequencies are then

$$f = \frac{\beta}{2\pi}\left(\frac{Hg}{\rho}\right)^{1/2}. \tag{6}$$

For the catenary of equation (3a), the hyperbolic terms in equation (4) vanish and equation (5) becomes $p_2 \equiv \beta$. Standard solutions for the catenary, equation (3a), and the beam, equation (3b), are readily available [6, 7].

Solutions for natural frequencies are obtained by applying appropriate boundary conditions on equation (4), to determine the constants A–D in terms of β and solving the resulting frequency equations for roots β_i. For the beam and bridge the boundary conditions of end curvature and/or slope are applied. For bridge symmetric modes it is also necessary to consider the effect of the tower and backstay via a boundary condition linking longitudinal motion of the cable and oscillating main cable tension. The mode shapes for mode i, $\varphi_i(x)$, are particular forms of equation (4) obtained by substituting for β_i.

The solutions for frequency and mode shape are given in Appendix A and the particular values of frequency obtained with the design values are given in Table 1 for the first antisymmetric mode (denoted as VA1 with natural frequency f_{VA1}) and the first symmetric mode (denoted as VS1 with natural frequency f_{VS1}).

Values in the column labelled $v'' = k_r v'$ are obtained when the uncertain fixity at each deck end is represented by a variable rotational restraint k_r corresponding to a rotational spring $k_\theta = k_r EI$. A value $k_r = 1{\cdot}0$ was assumed initially, there being no direct way to measure this value. The pinned and clamped conditions correspond to $k_r = 0$ and $k_r = \infty$.

4.1. ANTISYMMETRIC MODES

In Figure 2 are shown the mode shapes corresponding to the frequencies given in Table 1; modes for the pinned beam, bridge or catenary are indistinguishable from each other, as are the two clamped modes. For the same end fixity the bridge natural frequencies are only slightly higher than for beam alone. The cable makes little contribution to the bridge dynamic stiffness as it is relatively flexible for the antisymmetric modes, which are essentially beam vibration modes. The antisymmetry implies zero variation of cable tension and hence no deflection of the tower, so (to first order) the backstay is not a factor in these modes.

4.1. SYMMETRIC MODES

The symmetric modes have more complex solutions since, unlike antisymmetric modes, there will be significant cable stretching and oscillating tension h.

In Figure 3 are shown the mode shapes corresponding to the frequencies given in Table 1. The much increased stiffness of the combination (the top three values and shapes in Figure 3) as compared to either beam or catenary on their own (the lower three values and shapes in Figure 3) is because the cable is forced into a zero-node pattern, which requires significant cable stretching over the natural double-node pattern for cable alone.

5. DISCRETIZED (FINITE ELEMENT) MODEL

The same parameters were used in a two-dimensional (2-D) FE model developed [8] to explore non-linear effects in suspension bridges. Frequencies for VS1 and VA1 for

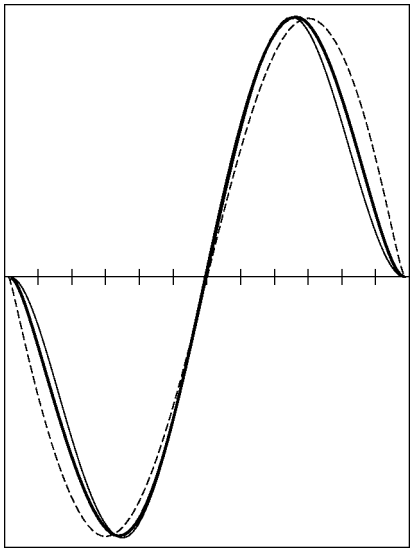

Figure 2. The antisymmetric vibration modes for catenary, beam and bridge. – – –, 1·654 Hz, pinned; 1·585 Hz, pinned beam; 0·472 Hz, cable. ——, 2·528 Hz, clamped; 2·476 Hz, clamped beam. —— 2·313 Hz, $k_r = 1{\cdot}0$.

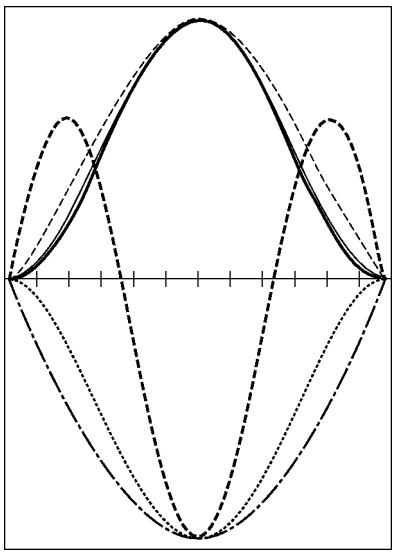

Figure 3. The symmetric vibration modes for cantenary, beam and bridge. – – –, 1·682 Hz, pinned; ——, 1·750 Hz, $k_r = 1{\cdot}0$; ▬, 1·771 Hz, clamped; – – –, 0·672 Hz, cable; –·–·–, 0·396 Hz, pinned beam; ·····, 0·898 Hz, clamped beam.

the same end conditions used in the DP model ($k_r = 0$, $k_r = 1$ and $k_r = \infty$) are given in Table 1.

In the FE model the mass is lumped at the nodes, which are at the connections between hangers and the deck or cables, together with tower base and tip and the backstay anchorage. The stiffness matrix $\mathbf{K}$ comprises an elastic component $\mathbf{K}_e$ and a geometrically non-linear gravity stiffness $\mathbf{K}_g$ due to the axial loads in cables and hangers. Although for this bridge the hangers are stiff, the model allows for hangers that do not take axial compressive loads. As in the DP model, the FE representation collapses the two cable planes into one. The model has only 33 degrees of freedom.

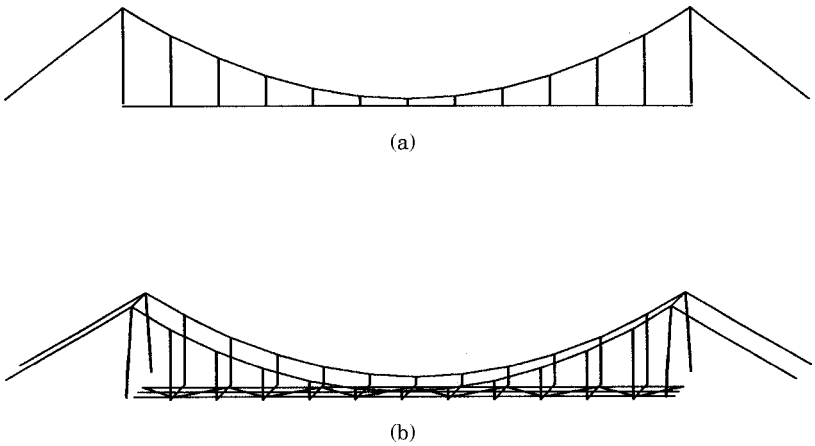

Figure 4. Equivalent finite element models for the vertical plane response: (a) two-dimensional (2-D); (b) three-dimensional (3-D).

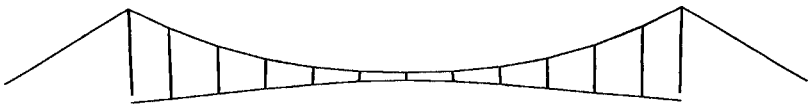

Mode VS1, 1.634 Hz

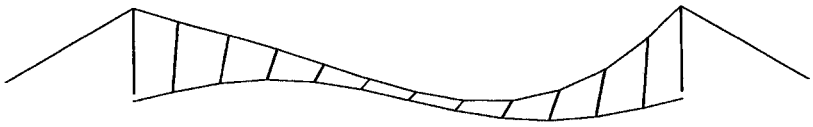

Mode VA1, 1.655 Hz

Mode LS1, 1.644 Hz

Mode TS1, 2.753 Hz

Mode TA1, 4.477 Hz

Figure 5. Modes predicted by the 3-D FE model (from design data with $k_r = 0$).

As a check on the accuracy of the 2-D model in representing a three-dimensional structure, a full three-dimensional (3-D) model was set up using SAPIV and ANSYS codes. The 3-D mesh and the equivalent 2-D mesh are shown in Figure 4. Some mode shapes generated by the 3-D solution for the pinned deck condition ($k_r = 0$) are shown in Figure 5: modes VS1 and VA1 together with the fundamental lateral and torsional modes LS1 and TS1 are shown. As there is minimal difference between vertical modes from 3-D and 2-D solutions (even for more complex multi-noded mode shapes), the simple 2-D model is used in the correlation.

The 2-D FE frequencies are close enough to the DP frequencies for the models to be used in parallel. While values of either f_{VA1} or f_{VS1} are almost the same between the DP and FE models, both are far too low compared with experimental estimates, showing the need to modify the parameters in the models. The effects of varying structural parameters were explored using both models.

The parameters length (l), sag (d), horizontal tension (H), load (ρ) and backstay length (l_s) are known accurately, leaving the following uncertainities: (1) I for the deck, since no account is made for handrail or other steelwork; (2) E_c for the main cable and backstay, since the design value is rather conservative; and (3) the rotational constraint k_r at the deck end. These are seen as independent parameters in the frequency equations (Appendix A).

Updating of three parameters in a model via system identification requires experimental measurement of at least three values. A prototype test was conducted to determine a set of at least three natural frequencies and mode shapes.

6. PROTOTYPE TESTING

The preliminary testing that highlighted the peculiar response at 2 Hz also showed the need for a form of prototype testing able to define clearly the modal characteristics of the bridge. Hammer testing [9] was used, being an ideal method for a structure of this size and having several advantages over other possible methods; the equipment is simple and portable, requiring no mains power supply, and each impact provides a wide-band load with a good signal to noise ratio in the response, so that the frequency response function (FRF) between excitation and response points can be determined with just a few hammer blows.

Some factors that improve the quality of data obtained from prototype testing are as follows: (1) high quality accelerometers should be used, having a response signal well above instrument noise; (2) low-pass filters should be used to remove unwanted high amplitude high frequency transients, in order to obtain the maximum benefit from the recorder/analyzer dynamic range; (3) the force (transient)/response (exponential) windows should be used carefully to minimize ambient noise effects.

In this test, a 16 lb (7·25 kg) instrumented hammer, an amplifier and low-pass filter (Dytran), a pair of accelerometers (Allied Signal QA-700) with home-built signal conditioning, a DAT tape recorder (TEAC RD120) and a dual channel signal analyzer (Brüel and Kjær 2148) were used.

Although lateral and torsional modes were measured, the main concern was vertical modes, measured on the deck, by maintaining one accelerometer at the same position and moving the hammer to each of the 11 locations corresponding to hanger terminations and transom beams.

The FRF, as a function of frequency ω measured between the acceleration response at position $b(\ddot{x}_b)$ and the force at position $a(p_a)$ is the inertance function

$$I(\omega) = \frac{\ddot{x}_b}{p_a} = \sum_i \frac{-\omega^2 \varphi_{ia} \varphi_{ib}}{m_i(\mathrm{w}_\mathrm{i}^2 - \omega^2 + 2\mathrm{j}w\omega_i\zeta_i)}, \tag{7}$$

in which m_i, ω_i and ζ_i are, respectively, the modal mass, the frequency and the damping ratio for mode i.

Because of reciprocity, in theory there is no difference between moving the hammer (varying a) and moving the accelerometer (varying b). In practice, the moving mass of the tester may result in slight modifications to the modal parameters.

Data were analyzed on a 0–25 Hz base-band, with 801 lines and 0·0312 Hz resolution. Force (0·2 s duration T_F) and response (4 s time constant T_R) windows were used, taking an average of four hammer impacts.

As well as hammer testing, modes VS1 and VA1 were excited by jumping followed by free decay, in order to provide damping estimates directly from the logarithmic decrement. Finally, the response due to a single pedestrian crossing the bridge was recorded.

7. EXPERIMENTAL MODAL CHARACTERISTICS

A set of 11 FRFs, corresponding to each of the measurement locations, were analyzed using both ICATS [10] and MDOF [11] modal analysis software. The imaginary component of $I(\omega)$ (see Figure 6) clearly shows the presence of two very close modes, in antiphase for this particular combination of positions a and b.

In Figure 7 are shown measured mode shapes (φ_{ia}) for the lowest five measured modes ($i = 1, \ldots, 5$) and 11 excitation positions (a) together with frequencies and damping ratios. In Figure 6 a sixth mode is indicated at approximately 11·1 Hz, which has a mode shape that is almost indistinguishable from that of mode VS3 and which was not generated in any of the models.

Damping ratio estimates ζ_{est} for the three higher modes were obtained from ICATS with a correction for the effect of the response window: $\zeta_{est} = \zeta_{\mathrm{ICATS}} - 1/2\pi f T_R$. Values ζ_{est} for the fundamental symmetric and antisymmetric modes were obtained from the tail ends of the free decay response from large oscillations induced by jumping.

In Figure 8 are shown values of ζ obtained for mode VA1 via logarithmic decrement. The values decrease from 1·8% for a peak-to-peak 1/4 span amplitude of 35 mm to 1% at low amplitude. Likewise, for VS1 the lowest value obtained was 1%.

8. TORSIONAL AND LATERAL RESPONSE

Measurements of the lateral and torsional response were made for reference but, as mentioned previously, the modes were not so easily excited and therefore not a critical concern.

Two torsional modes were identified; an antisymmetric mode (TA1) at 1·84 Hz with approximately 2·4% damping and a symmetric mode (TS1) at 2·52 Hz with approximately 1·4% damping. The fundamental lateral mode (LS1) at 1·25 Hz was found to be symmetric and very heavily damped.

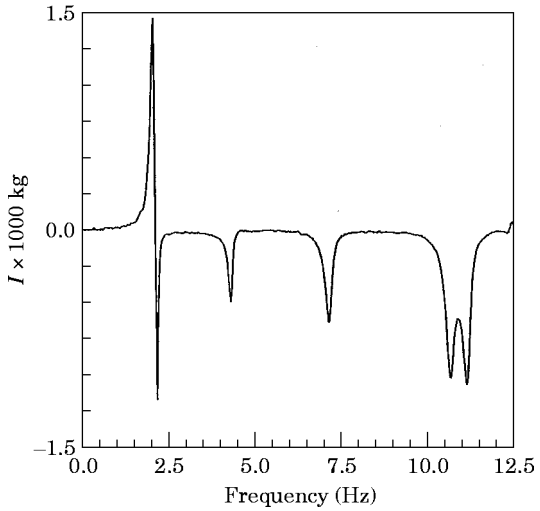

Figure 6. The imaginary part of inertance function $I(\omega)$.

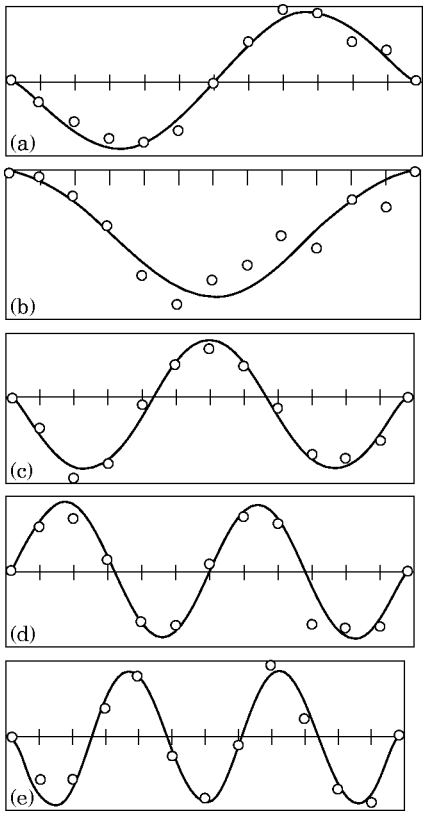

Figure 7. A comparison of theoretical mode shapes from the DP model with experimental values (circles). (a) Mode VA1: $f_{VA1} = 2{\cdot}072$ Hz, $\zeta_{VA1} \sim 1{\cdot}0\%$, MAC $= 0{\cdot}976$. (b) Mode VS1: $f_{VS1} = 2{\cdot}151$ Hz, $\zeta_{VS1} \sim 1{\cdot}0\%$, MAC $= 0{\cdot}955$. (c) Mode VS2: $f_{VS2} = 4{\cdot}288$ Hz, $\zeta_{VS2} = 2{\cdot}0\%$, MAC $= 0{\cdot}978$. (d) Mode VA2: $f_{VA2} = 7{\cdot}136$ Hz, $\zeta_{VA2} = 1{\cdot}32\%$, MAC $= 0{\cdot}928$. (e) Mode VS3: $f_{VS3} = 10{\cdot}631$ Hz, $\zeta_{VS3} = 1{\cdot}56\%$, MAC $= 0{\cdot}964$.

Comparison with the 3-D solution (Figure 5) shows reasonable agreement for LS1. In fact, assuming no restraint on rotation about a vertical axis at the deck ends, the mode LS1 frequency depends heavily on the effectiveness of the diagonal bracing.

The 3-D model collapses the stringers, transoms, diagonal bracing and handrail into a horizontal plane, which undervalues the rotational inertia and over-emphasizes the stiffness of the steel frame and its connections in torsion, so the predicted TA1 and TS1 frequencies are bound to be too high. Even so, it is surprising that the antisymmetric modes TA1 appears at the lower frequency.

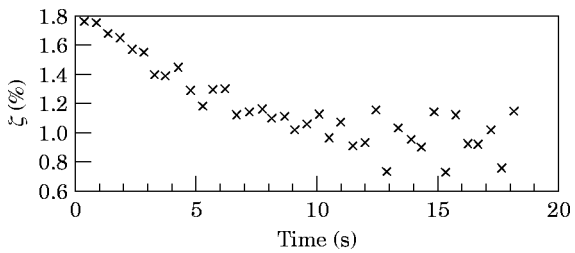

Figure 8. Damping values for mode VA1 obtained by logarithmic decrement during free decay.

9. SYSTEM IDENTIFICATION

Based on the initial theoretical estimates and the measured natural frequencies, the parameters I, E_c and k_r were adjusted to obtain a good fit between the experimental values for the first five vertical mode natural frequencies and those obtained from the 2-D FE model.

The least squares procedure [12] was used, as follows. If the prior estimates of structural parameters (I, E_c and k_r) are assembled into a column vector $\mathbf{r}_0$, the FE values of natural frequencies obtained using $\mathbf{r}_0$ are written as a column vector $\mathbf{y}_0$ and the experimental (exact) values of natural frequency are written as $\mathbf{y}_e$, then for small differences between experimental and FE values the "correct" values of the parameters $\mathbf{r}$ are found using

$$\mathbf{y}_0 - \mathbf{y}_e = \mathbf{T}(\mathbf{r}_0 - \mathbf{r}) \tag{8}$$

or $\mathbf{Y} = \mathbf{TR}$, where $\mathbf{T}$ is a sensitivity matrix with terms $\partial y_k/\partial r_i$, $i = 1, \ldots, 3$, $k = 1, \ldots, 5$. The iteration scheme to find $\mathbf{r}$ via $\mathbf{R} = \mathbf{T}^{-1}\mathbf{Y}$ becomes

$$\mathbf{r}_{n+1} = \mathbf{r}_n - \mathbf{T}^{-1}(\mathbf{y}_n - \mathbf{y}_e). \tag{9}$$

Since $\mathbf{T}$ is a 5×3 matrix, the pseudo-inverse $(\mathbf{T}^{\mathrm{T}}\mathbf{T})^{-1}\mathbf{T}^{\mathrm{T}}$ was used, which is equivalent to a least squares minimization.

The effective cable area was maintained at 66% of solid value, i.e., 708 mm^2, while better starting values of E_c and k_r were used in the DP model based on the observations, from Table 1 and Appendix A, that f_{VS1} is too low and increases with E_c, while k_r, which affects f_{VA1}, lies somewhere between 0·0 and 1·0. Initial values in $\mathbf{r}_0$ were thus $E_c = 100$ kN/mm^2, $k_r = 0{\cdot}3$ and $I = 1{\cdot}020 \times 10^8$ mm^4.

After three iterations with equation (9), each requiring four eigensolutions (to determine $\mathbf{T}$ and the updated $\mathbf{y}$), $\mathbf{r}$ converged to $E_c = 100{\cdot}43$ kN/mm^2, $k_r = 0{\cdot}2474$ and $I = 1{\cdot}1336 \times 10^8$ mm^4.

In Table 2 the natural frequencies ($\mathbf{y}$) using these values are compared with the experimental frequencies and values obtained with equations (A7) and (A14).

The last three columns show the elements of $\mathbf{T}$ as $100(r_i/\lambda_k)(\partial\lambda_k/\partial r_i)$, representing the percentage change in mode frequency per 100% change in parameter. Clearly, E_c is the dominant parameter in mode VS1, for which k_r has little effect. E_c has a much smaller influence on other symmetric modes. The girder rigidity I is the dominant parameter for all other modes, and to a lesser extent k_r.

The mode shapes obtained from equations (A6) and (A14) using values in column 4 of Table 2 are shown as the smooth curves in Figure 7. The Modal Assurance Criterion (MAC) values in Figure 7 relate to the closeness of fit between experimental mode shape values and the corresponding mode shapes values from equations (A6) and (A14) for the exact measurement points.

TABLE 2

Adjusted theoretical natural frequencies (f) and sensitivities ($\mathbf{T}$)

Mode	Experimental value (Hz)	FE value (Hz)	DP value (Hz)	$\partial f/\partial E_c$ (%)	$\partial f/\partial I$ (%)	$\partial f/\partial k_r$ (%)
VA1	2·072	2·110	2·142	0·00	**46·24**	11·39
VS1	2·151	2·149	2·146	**39·70**	7·58	0·60
VS2	4·288	4·300	4·412	2·89	**44·78**	8·07
VA2	7·136	7·059	7·298	0·01	**47·32**	6·22
VS3	10·631	10·672	11·115	0·09	**48·25**	5·08

10. SIMULATION OF PEDESTRIAN RESPONSE TIME HISTORIES

In its context as part of a tourist attraction, the bridge exhibits acceptable behaviour for its users. Its liveliness is not a problem—it is a feature. Where liveliness is not desirable, particularly in a more conventional footbridge having a low fundamental natural frequency (f_0), consideration is usually given to vibration serviceability defined in terms of objective criteria [13–15] for pedestrian comfort.

If pedestrian comfort is an issue, the applicable code in Singapore, BS5400 [13], specifies a vibration limit $0{\cdot}5(f_0)^{1/2}\,\mathrm{m\,s^{-2}}$ for a single pedestrian, but apparently [15] this is only a recommendation. BS5400 also provides a method of calculating response by approximating a pedestrian as a pulsating dynamic load,

$$F(t) = 180 \sin (2\pi f_0 t)N, \tag{10}$$

moving across the bridge at a speed of $0{\cdot}9f_0$ m/s, using the appropriate specified logarithmic decrement δ, which is 0·03 (for steel with asphalt or epoxy surfacing).

The forces generated during walking (running and jumping) are not pure sinusoids and can be modelled as Fourier series of the form [15]

$$F(t) = P\left(1 + \sum_{n=1}^{N} \alpha_n \sin (2\pi nft + \varphi_n)\right), \tag{11}$$

in which the fundamental ($n = 1$) is the strongest with $\alpha_1 \approx 0{\cdot}35$ for $f \approx 2$ Hz, giving a pulsating force of 294 N for a 75 kg person ($P = 736$ N). Equation (10) is equivalent to equation (11) if only the first term is taken, with $\alpha_1 = 0{\cdot}24$.

It is probable that α_1 would be higher if the subject was deliberately walking heavily to excite the bridge; for jumping, α_1 can be as high as 1·75. Also the value $\delta = 0{\cdot}03$ ($\zeta \approx 0{\cdot}5\%$) is too low, since from measurements $\zeta \geqslant 1\%$.

For the DP model, the response is obtained by normal mode analysis, writing

$$v(x, t) = \sum_i \varphi_i(x) Y_i(t). \tag{12}$$

Using equation (3c), with $\rho' = \rho/g$ and constant member properties,

$$\ddot{v}\rho' - Hv'' + EIv^{iv} - 8dh/l^2 = F\delta(x - vt) \sin 2\pi ft. \tag{13}$$

The modal response (mode i) is then obtained from

$$\ddot{Y}_i \int_{-1/2}^{1/2} \rho' \varphi_i^2 \, \mathrm{d}x + Y_i \int_{-1/2}^{1/2} [-H\varphi_i'' \varphi_i + EI\varphi_i^{iv} \varphi_i - 8d\hat{h}/l^2 \varphi_i] \, \mathrm{d}x = F\varphi_i(vt) \sin (ft). \tag{14}$$

The first integral is the modal mass m_i and the second is the modal stiffness k_i ($= m_i\omega_i^2$), for mode i. Adding a damping term,

$$m_i(\ddot{Y}_i + 2\zeta_i\omega_i\dot{Y}_i + \omega_i^2 Y_i) = F\varphi_i(vt) \sin 2\pi ft. \tag{15}$$

For the first pinned antisymmetric mode ($h = 0$, $\varphi_1(x) = \sin 2\pi x/l$),

$$\frac{\rho' L}{2}(\ddot{Y} + 2\zeta\omega\dot{Y} + \omega^2 Y) = F \sin \frac{2\pi vt}{l} \sin 2\pi ft. \tag{16}$$

Variations of equation (16) with different modal mass and more complex functions $\varphi_i(x)$ (as in Appendix A) to replace $\sin(2\pi vt/l)$ will apply to other end conditions and symmetric modes, and the response for two modes together can be obtained by superposition.

The response to a moving pedestrian was simulated first using VS1 and VA1 mode shapes from Appendix A in a Duhammel integral with equation (16) and, second, using the non-linear FE model with $\alpha_1 = 0{\cdot}35$ and $\zeta = 1\%$. The following peak acceleration values (m/s^2) were obtained:

	1/4 span	Mid-span	3/4 span
DP	3·34	3·09	3·34
FE	2·71	2·55	2·28
FE + m_t	2·42	2·28	2·19

The measured maximum value (at 3/4 span) was 2·18 m/s^2.

The last row in the above table is for a non-linear simulation in which the mass m_t of the pedestrian accelerating at $\ddot{v}_t$ is added in as a forcing term $-m_t\ddot{v}_t$. For the FE simulations the walking frequency is taken as the average of f_{VA1} and f_{VS1}.

It is worth noting that for all but the largest amplitude oscillations [8] the vertical plane vibrations of a suspension bridge with invariant mass are well represented by models linearized about the dead load condition. The most significant non-linearities are likely to come from the various mechanisms that constitute "structural damping" [16].

In Figure 9 is shown the actual acceleration response measured with a pedestrian (a 75 kg student tester) walking briskly and heavily across the bridge in the direction from 1/4 span to 3/4 span, and in Figure 10 are shown the acceleration time histories generated

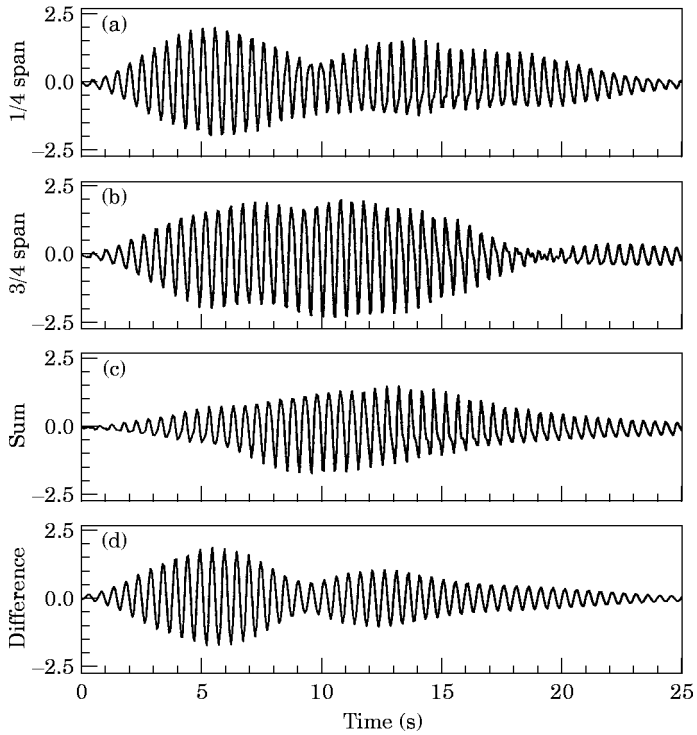

Figure 9. The measured vibration acceleration response (in m/s^2) due to the passage of a "pedestrian".

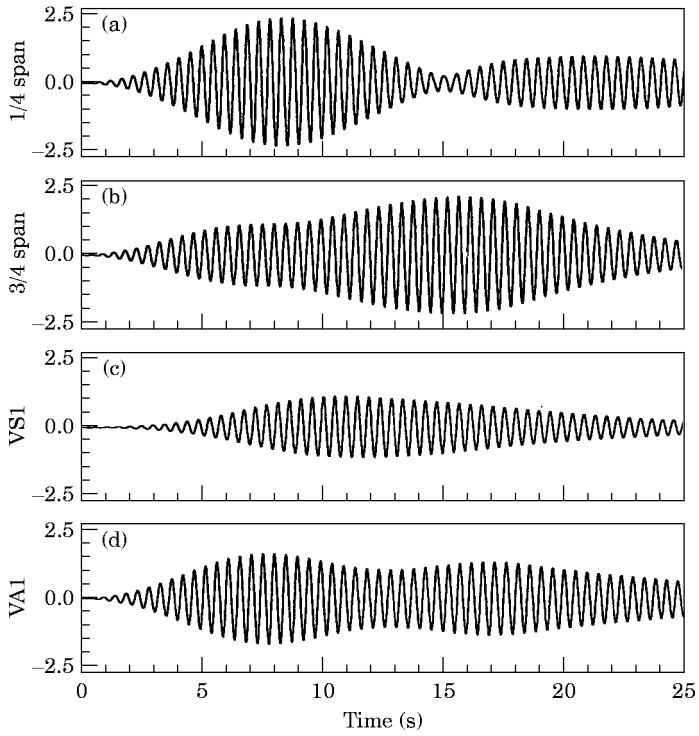

Figure 10. The simulated vibration acceleration response (in m/s^2) due to the passage of a "pedestrian".

in the non-linear simulation (FE + m_t). Figures 9(a) and 10(a) are for 1/4 span responses, and Figures 9(b) and 10(b) are for 3/4 span responses. Figures 9(c) and 10(c) and Figures 9(d) and 10(d) are, respectively, the half-sum and half-difference of the 1/4 span and 3/4 span, intended to represent the responses in mode VS1 and mode VA1 respectively. Comparison of Figures 9 and 10 suggests an underestimation of damping and walking speed (i.e., stride) in the simulation.

Note that since the response is almost entirely due to 2 Hz modes, the accelerations can be converted approximately to displacements (in mm) by multiplying by $1000/\omega^2 \approx 6{\cdot}3$.

None of the simulations consider the variable damping (Figure 9) or the flexibility and damping capacity of the pedestrian. In the DP simulation, f_{VA1} and f_{VS1} are practically identical and the response is dominated by mode VS1 response.

11. DISCUSSION AND CONCLUSIONS

Simple two-dimensional finite element (FE) and distributed parameter (DP) models can be used to study the dynamics of the critical vertical plane response of the bridge and produce very similar estimates of bridge modes. Depending on computer implementation (these models were run on a PC) the FE model has the slight advantage in terms of ease of studying the effect of different parameters on several modes at once.

The DP model is very useful for predicting f_{VS1} and f_{VA1} alone. From studying these results it is clear that the cable axial stiffness is most important for the first symmetric mode (VS1), and apart from this the other modes are similar to those of a beam with partially fixed ends. This is reflected in the FE system identification sensitivity matrix.

The coincidence of f_{VS1} and f_{VA1} at a typical footfall frequency accounts for the relatively high response of the bridge despite its conservative rigidity. In usual usage, the passage of several pedestrians would reduce the additive effect of modes and alter the dynamic characteristics. When modelling the response to a pedestrian, the response depends very much on the closeness of the two modes and the walking characteristics.

The issue of serviceability is of course very important for this type of bridge. Clearly, it is lively, and since part of its function is to induce tourists to come and enjoy its bouncy behaviour, it is definitely serviceable.

Were it desirable, tuning of the bridge to adjust vertical plane natural frequencies upwards or downwards could be done via the girder rigidity and cable stiffness. Another parameter is the length of backstay, which would affect mode VS1 the most. For an existing bridge, frequencies could be altered by adjusting handrail continuity at deck ends, or by adding mass at strategic points. The use of discrete dampers [15] would probably be less viable for this type of bridge, since they would require maintenance.

12. ACKNOWLEDGMENTS

The author wishes to thank NTU final year students Kho Chza-Main and Chin Yong-Pheng for the very capable execution of the experimental work, Dr Cheng Wen-Haur, Mr B. Harrison and Mr M. Graetz of Singapore Zoological Gardens for their assistance, and Mr P. Chalk of Works Consultancy for providing the design information.

REFERENCES

1. R. L. Pimentl, P. Waldron and W. J. Harvey 1995 *Analysis and Testing of Bridges*. *Joint SECED/I. Struct*. *E Seminar*, *Institute of Structural Engineers London*, 26 *April*. Assessment of the dynamic behaviour of Aberfeldy glass reinforced plastic cable-stayed footbridge.
2. J. M. W. Brownjohn, A. A. Dumanoglu and C. A. Taylor 1994 *Engineering Structures* **16**, 401–415. Dynamic investigation of a suspension footbridge.
3. J. M. W. Brownjohn, A. A. Dumanoglu, R. T. Severn and C. A. Taylor 1987 *Proceedings*, *Institution of Civil Engineers*, *Part* 2 **83**, 561–600. Ambient vibration measurements of the Humber Suspension Bridge and comparison with calculated characteristics.
4. J. M. W. Brownjohn, A. A. Dumanoglu, R. T. Severn and A. Blakeborough 1989 *Earthquake Engineering and Structural Dynamics* **18**, 263–283. Ambient vibration survey of the Bosporus Suspension Bridge.
5. J. M. W. Brownjohn, A. A. Dumanoglu and R. T. Severn 1989 *Earthquake Engineering and Structural Dynamics* **21**, 907–924. Ambient vibration survey of the Fatih Sultan Mehmet (Second Bosporus) Suspension Bridge.
6. H. M. Irvine and T. K. Caughey 1974 *Proceedings of the Royal Society*, *London* **A341**, 299–315. The linear theory of the free vibration of a suspended cable.
7. R. D. Blevins 1979 *Formulas for Natural Frequency and Mode Shape*. New York: Krieger.
8. J. M. W. Brownjohn 1994 *Earthquake Engineering and Structural Dynamics* **23**, 1351–1367. Observations on non-linear dynamic characteristics of suspension bridges.
9. J. R. Maguire 1984 *Ph.D*. *Thesis*, *University of Bristol*, *Department of Civil Engineering*. Assessing the dynamic properties of prototype structures by hammer testing.
10. Imperial College of Science, Technology and Medicine, London *MODENT Reference Manual*. Imperial College Analysis Testing and Software.
11. J. M. W. Brownjohn 1992 *Earthquake Engineering Research Centre*, *University of Bristol*, *TI* 23008. Modal analysis of MDOF systems with particular reference to base excitation.
12. J. D. Collins, G. C. Hart, T. K. Hasselman and B. Kennedy 1974 *American Institute of Aeronautics and Astronautics Journal* **12,** 185–190. Statistical identification of structures.
13. British Standards Institution 1978 *Steel*, *Concrete and Composite Bridges*. *Part* 2. *Specification for Loads*. *BS*5400: *Part* 2: 1978.
14. J. H. Rainer, G. Pernica and D. E. Allen 1988 *Canadian Journal of Civil Engineering* **15**, 66–71. Dynamic loading and response of footbridges.

15. R. T. JONES, A. J. PRETLOVE and R. EYRE 1981 *The Structural Engineer* **59B**, 27–32. Two case studies in the use of tuned vibration absorbers on footbridges.
16. J. M. W. BROWNJOHN 1994 *Proceedings, Institution of Civil Engineers, Structures and Buildings* **104**, 401–415. Estimation of damping in suspension bridges.

APPENDIX A: NATURAL FREQUENCIES AND MODE SHAPES FROM CONTINUUM EQUATIONS

The starting point in determining frequencies and mode shapes is the solution of equation (3c):

$$\hat{v}(x) = A \cosh(p_1 x) + B \sinh(p_1 x) + C \cos(p_2 x) + D \sin(p_2 x) - 8d\hat{h}/(\beta l)^2 H. \quad \text{(A1)}$$

A.1. ANTISYMMETRIC MODES

For antisymmetric modes, symmetry requires that $A = C = \hat{h} = 0$, leaving

$$\hat{v}(x) = B \sinh(p_1 x) + D \sin(p_2 x). \quad \text{(A2)}$$

Pinned girder. The boundary conditions are $v(\pm l/2) = v''(\pm l/2) = 0$, leading to $B = 0$ and a frequency equation

$$\sin(p_2 l/2) = 0 \quad \text{(A3)}$$

with mode shapes, for unit D and values of p_2 satisfying equation (A3), of

$$\varphi(x) = \sin(p_2 x). \quad \text{(A4)}$$

Clamped girder. The boundary conditions are $v(\pm l/2) = v'(\pm l/2) = 0$, leading to a frequency equation

$$\tan(p_2 l/2) = (p_2/p_1) \tanh(p_1 l/2) \quad \text{(A5)}$$

with mode shapes, for unit D and β satisfying equation (A5), of

$$\varphi(x) = \sin(p_2 x) - \frac{\sin(p_2 l/2)}{\sinh(p_1 l/2)} \sinh(p_1 x). \quad \text{(A6)}$$

Girder with rotational springs. The boundary conditions are $v(\pm l/2) = 0$, $v''(-l/2) = k_r v'(-l/2)$, $v''(l/2) = -k_r v'(l/2)$, with $k_r = k_\theta/EI$, leading to a frequency equation

$$p_2 \cot(p_2 l/2) - p_1 \coth(p_1 l/2) = \frac{(1+\varepsilon)^{1/2}}{\alpha k_r}, \quad \text{(A7)}$$

with mode shapes given by equation (A6) for β satisfying equation (A7).

Equations (A3) and (A5) are special cases of equation (A7) when, respectively, $k_r = 0$ and $k_r = \infty$.

A.2. SYMMETRIC MODES

For symmetry, B, $D = 0$, but the oscillating component of tension $\hat{h}$ is not required to be zero; i.e.,

$$\hat{v}(x) = A \cosh(p_1 x) + C \cos(p_2 x) - 8d\hat{h}/(\beta l)^2 H. \quad \text{(A8)}$$

Solutions are more complex than for the antisymmetric modes, since cable stretching due to the non-zero $\hat{h}$ has to be taken into account via the "cable equation" [6], which in this case leads to

$$\frac{\hat{h} l_e}{E_c A_c} = [\hat{u}]_{-l/2}^{+l/2} - \int_{-l/2}^{+l/2} y'' \hat{v} \, \mathrm{d}x \quad \text{(A9)}$$

where the "virtual cable length" $l_e \approx l(1 + 8(d/l)^2)$, E_c and A_c are the cable modulus and sectional area, and $\hat{u}(x)$ is the longitudinal deflection.

The frequency equations are obtained by determining A and C in equation (A8) in terms of $\hat{h}$ via the boundary conditions and then substituting equation (A8) into equation (A9). In addition, the effect of the backstay length l_s and inclination θ can be approximated by a spring $k_s = E_c A_c \cos^2\theta/l_s$ such that

$$\hat{u}(l/2) - \hat{u}(-l/2) = 2\hat{h}/k_s. \tag{A10}$$

Pinned girder:

$$\frac{(\beta l)^2}{\lambda^2}\left\{1 + \frac{2l_s}{\cos^2\theta l_e}\right\} = 1 - \left(\frac{2}{p_2 l}\right)\frac{[\tan(p_2 l/2) + (p_2/p_1)^3 \tanh(p_1 l/2)]}{(1 + (p_2/p_1)^2)}, \tag{A11}$$

where

$$\lambda^2 = E_c \frac{A_c}{H}\frac{l}{l_e}\left(\frac{8d}{l}\right)^2.$$

Clamped girder:

$$\frac{(\beta l)^2}{\lambda^2}\left\{1 + \frac{2l_s}{\cos^2\theta l_e}\right\} = 1 - \left(\frac{2}{p_2 l}\right)\frac{(1 + (p_2/p_1)^2)}{[\cot(p_2 l/2) + (p_2/p_1)\coth(p_1 l/2)]}. \tag{A12}$$

Girder with rotational springs:

$$\frac{(\beta l)^2}{\lambda^2}\left\{1 + \frac{2l_s}{\cos^2\theta l_e}\right\} = 1 - \left(\frac{2}{p_2 l}\right)\frac{(\sin(p_2 l/2) + (p_2/p_1)\gamma \sinh(p_1 l/2))}{(\cos(p_2 l/2) + \gamma \cosh(p_1 l/2))}, \tag{A13}$$

where

$$\gamma = \left(\frac{p_2}{p_1}\right)\frac{(k_r \sin(p_2 l/2) + p_2 \cos(p_2 l/2))}{(k_r \sinh(p_1 l/2) + p_1 \cosh(p_1 l/2))}.$$

Equations (A11) and (A12) are special cases of equation (A13) when, respectively, $k_r = 0$ and $k_r = \infty$.

Mode shapes for the symmetric modes are given by using appropriate values of γ and β satisfying equations (A11)–(A13):

$$\varphi(x) = \frac{8d\hat{h}}{(\beta l)^2}\left\{\frac{\cos(p_2 x) + \gamma \cosh(p_1 x)}{\cos(p_2 l/2) + \gamma \cosh(p_1 l/2)} - 1\right\}. \tag{A14}$$

For a catenary with fixed ends, $l_s = 0$, $p_2 = \beta$ and $\gamma = 0$, and then equations (A11)–(A13) lead to the frequency equation

$$\left(\frac{\beta l}{2}\right)^2 \frac{4}{\lambda^2} = 1 - \left(\frac{2}{\beta l}\right)\tan\left(\frac{\beta l}{2}\right). \tag{A15}$$

Finally, in the symmetric mode, the tower tip displacement is related to the mid-span displacement by

$$\hat{u}(-l/2) = \varphi(0)\,\frac{H\beta^2 l_s}{E_c A \rho_c \cos^2\theta}\,\frac{1+\gamma}{(\cos(p_2 l/2) + \gamma\cosh(p_1 l/2))}\,. \tag{A16}$$